

## Optical Molecular Imaging of Epidermal Growth Factor Receptor Expression to Improve Detection of Oral Neoplasia<sup>1</sup>

Nitin Nitin<sup>\*,2</sup>, Kelsey J. Rosbach<sup>†,2</sup>, Adel El-Naggar<sup>‡</sup>, Michelle Williams<sup>‡</sup>, Ann Gillenwater<sup>‡</sup> and Rebecca R. Richards-Kortum<sup>†</sup>

\*Southwest Research Institute, San Antonio, TX, USA; <sup>†</sup>Rice University, Houston, TX, USA; <sup>‡</sup>MD Anderson Cancer Center, Houston, TX, USA

### Abstract

**BACKGROUND:** The development of noninvasive molecular imaging approaches has the potential to improve management of cancer. **METHODS:** In this study, we demonstrate the potential of noninvasive topical delivery of an epidermal growth factor–Alexa 647 (EGF–Alexa 647) conjugate to image changes in epidermal growth factor receptor expression associated with oral neoplasia. We report a series of preclinical analyses to evaluate the optical contrast achieved after topical delivery of EGF–Alexa 647 in a variety of model systems, including cells, three-dimensional tissue cultures, and intact human tissue specimens using wide-field and high-resolution fluorescence imaging. Data were collected from 17 different oral cancer patients: eight pairs of normal and abnormal biopsies and nine resected tumors were examined. **RESULTS:** The EGF-dye conjugate can be uniformly delivered throughout the oral epithelium with a penetration depth exceeding 500  $\mu\text{m}$  and incubation time of less than 30 minutes. After EGF–Alexa 647 incubation, the presence of oral neoplasia is associated with a 1.5- to 6.9-fold increase in fluorescence contrast compared with grossly normal mucosa from the same patient with both wide-field and high-resolution fluorescence imaging. **CONCLUSIONS:** Results illustrate the potential of EGF-targeted fluorescent agents for *in vivo* molecular imaging, a technique that may aid in the diagnosis and characterization of oral neoplasia and allow real-time detection of tumor margins.

*Neoplasia* (2009) 11, 542–551

### Introduction

Noninvasive, molecular-specific imaging has the potential to improve management of oral neoplasia by allowing characterization of specific molecular alterations, facilitating the individualized selection of therapy, and enabling real-time evaluation of treatment response [1–5]. Genetic changes that occur during carcinogenesis lead to altered gene expression and protein levels compared with normal cells. A number of promising molecular biomarkers of early oral neoplasia have been identified [6–9], including several specific mutations and molecular abnormalities that occur during the transition from normal mucosa to dysplasia to invasive carcinoma [10–12]. These molecules can serve as biomarkers for early detection strategies and follow-up of high-risk individuals. Although these data herald a breakthrough for deciphering the mechanisms of oral carcinogenesis, they were obtained through analytical techniques requiring tissue from invasive biopsies or surgical resections. Unfortunately, there are currently no techniques available to rapidly screen for these changes at the point-of-care.

The clinical use of molecular imaging in cancer patients has focused primarily on positron emission tomography (PET). This uses fluorodeoxyglucose or 3'-deoxy-3'-<sup>18</sup>F-fluorothymidine as contrast agents to provide images with molecular information and is now routinely used for staging and assessment of treatment response in cancer

Abbreviations: DMSO, dimethylsulfoxide; EGFR, epidermal growth factor receptor; IHC, immunohistochemical; MFI, mean fluorescence intensity; PET, positron emission tomography

Address all correspondence to: Rebecca Richards-Kortum, PhD, Department of Bioengineering, Rice University, 6100 Main St, Houston, TX 77005. E-mail: rkortum@rice.edu

<sup>1</sup>This study was funded by the National Cancer Institute grant BRP R01CA103830. This material is also based on work supported by the National Institutes of Health under grant no. 5T32 GM008362.

<sup>2</sup>Both authors contributed equally to this work.

Received 16 January 2009; Revised 8 March 2009; Accepted 11 March 2009

Copyright © 2009 Neoplasia Press, Inc. All rights reserved 1522-8002/09/\$25.00  
DOI 10.1593/neo.09188

patients [13–15]. Although PET imaging has important clinical advantages, it has had a limited role in cancer screening and early detection because of its limited spatial resolution and cost associated with cyclotron and radioimaging facilities. An additional major drawback of PET is radiation exposure to the patient.

Optical imaging of tissue autofluorescence has emerged as a strategy for detection and diagnosis of oral lesions [16,17] and is favorable owing to its ability to image tissue with high spatial (<1  $\mu\text{m}$  lateral resolution) and temporal resolution (usually video rate) using low-cost, portable devices. However, performance of autofluorescence imaging systems does not always represent an improvement over common white light inspection [18]. Combined fluorescence diagnosis using both autofluorescence and 5-aminolevulinic acid-induced protoporphyrin IX fluorescence shows improved sensitivity and specificity over autofluorescence alone but cannot be performed as quickly [18,19]. Permeation of 5-aminolevulinic acid through mucosa is highly variable, especially in the presence of keratin, and as a result, keratinized oral lesions, especially those exhibiting hyperkeratosis, may be more difficult to diagnose [20].

An alternative approach is optical molecular imaging [21–24], which combines the advantages of molecular-specific imaging with the strengths of optical imaging. For clinical application, a successful optical molecular imaging strategy must solve several challenges: it must use a contrast agent that can be effectively and safely delivered to a target tissue *in vivo*, and it must yield images of tissue in real time with the desired spatial resolution and field of view, with a high signal-to-noise ratio. Optical imaging of fluorescent contrast agents has been used previously to discriminate cancer cells from normal cells, such as the chlorotoxin/Cy5.5 contrast agent [25]. Although this agent binds to multiple types of cancer cells, it is not specific for a single target.

The epidermal growth factor receptor (EGFR) is an established biomarker for the detection of oral neoplasia [26–29] and also has potential prognostic value [30]. Although EGFR is present in proliferating cells in normal tissue [31], there is marked overexpression during progression to dysplasia and cancer [32]. An estimated 50% to 98% of oral cancers overexpress EGFR [33–37]. The expression of EGFR was a strong prognostic indicator for overall and disease-free survival in patients with advanced head and neck squamous cell carcinoma enrolled in a radiotherapy study and was highly predictive for local-regional relapse but not distant metastases [38].

The goal of this study was to develop and evaluate the potential of a topically delivered optical contrast agent to image EGFR expression for use in the early detection of oral neoplasia. We report a series of preclinical analyses to assess the potential of topically delivered EGF–Alexa 647 for molecular imaging of oral neoplasia; we evaluate the resulting optical contrast achieved in cells, three-dimensional tissue cultures, paired clinically normal and abnormal biopsies, and surgically resected oral tumors. High-resolution fluorescence imaging was used in biopsy specimens to evaluate the ability of the contrast agent to be delivered throughout the epithelium and to quantitatively assess image contrast. Wide-field fluorescence imaging was used to assess the spatial heterogeneity of EGFR expression in resected tumors and to quantify the increase in fluorescence intensity of abnormal tissue. High-resolution and wide-field imaging of contrast provide complementary information that may be useful for a better classification of disease state, detection of disease margins, and understanding spatial heterogeneity of biomarker expression. Contrast values achieved in the tissue specimens were compared with the results

of histopathologic diagnosis and immunohistochemical (IHC) analysis of EGFR expression.

## Materials and Methods

### *Preparation of EGF–Alexa 647*

To prepare EGF–Alexa 647 conjugate, EGF peptide (Calbiochem, San Diego, CA) was labeled with Alexa 647–carboxylic ester (Invitrogen, Carlsbad, CA) and purified using size exclusion chromatography and dialysis. This two-step purification was used to completely remove free dye from the labeled peptide; purification was monitored by spectroscopy. Murine-derived recombinant EGF peptide was used for the studies in cells, tissue phantoms, and biopsies, and human-derived recombinant EGF peptide was used for the resected oral lesions. Control experiments (including cells and tissue phantoms) were performed to ensure these data could be combined.

### *Incubation and Imaging of Cells and Tissue Phantoms*

To demonstrate the specificity of EGF–Alexa 647–based contrast agent, we incubated two cell lines with the conjugate. The 1483 cells (provided by Dr. Lotan, MD Anderson Cancer Center) were selected as a representative EGFR-positive cell line, whereas MDA-MB-435 cells (ATCC, Manassas, VA) were selected as a representative EGFR-negative cell line. The cells were incubated with EGF–Alexa 647 (0.01 mg/ml) for 30 minutes at 37°C and imaged live using a Zeiss LSM 510 confocal microscope (excitation, 633 nm; emission filter band pass, 650–700 nm, Carl Zeiss, Inc., Thornwood, NY). To further demonstrate specificity of the contrast agent, 1483 cells were first blocked with 1% BSA for 30 minutes and then incubated for 1 hour on ice with equimolar amounts of both EGF–Alexa 647 and anti-EGFR antibody (monoclonal antibody clone 108, Baylor College of Medicine) labeled with Alexa 488 (Invitrogen, CA). In addition, a competition assay was performed in which 1483 cells were incubated for 1 hour on ice with EGF–Alexa 647 and unlabeled EGF. Incubation on ice was conducted to limit intracellular uptake of EGF receptors. The unlabeled EGF was added in concentrations of 0 $\times$ , 0.1 $\times$ , 1 $\times$ , and 10 $\times$  the molar concentration of EGF–Alexa 647. The 1483 cells were also incubated with rhodamine-labeled 3-kDa dextran, a nonspecific fluorescent agent with a similar size as EGF peptide does. Concentration and incubation conditions for cells with dextran were identical to cells with EGF–Alexa 647. Appropriate power and gain settings to image the rhodamine-labeled dextran with the confocal microscope were determined by first imaging a well with dextran that had not yet been washed and by adjusting the settings to detect a strong fluorescence signal from these wells. These settings were then used to image cells that were incubated with dextran and washed.

To assess the potential ability to topically deliver EGF–Alexa 647, a three-dimensional tissue culture system was used. Tissue phantoms were prepared by placing a suspension of approximately 10 million 1483 or 435 cells in a collagen matrix [39]. Phantoms were cultured for 24 hours in a cylindrical chamber (Costar Transwell Chambers; Corning, Lowell, MA) before subsequent incubation and imaging. The EGF-dye conjugate was topically delivered only to the top surface area of the tissue phantom (0.05 mg/ml). After 30 minutes of incubation, tissue phantoms were washed in excess medium to remove unbound contrast agent. After incubation, tissue phantoms were sliced transversely using a Krumdieck tissue slicer (Alabama Research & Development; 200–300  $\mu\text{m}$  thick) and imaged using a Zeiss LSM 510

confocal fluorescence microscope using the same settings used for cell imaging.

### Topical Delivery of EGF–Alexa 647 in Clinical Samples

To demonstrate the potential of EGF–Alexa 647 to detect oral neoplasia, the conjugate was topically applied to fresh tissue samples obtained from oral cancer patients. Paired sets of clinically normal and abnormal oral biopsies ( $n = 8$ ) were used initially to ensure translation of results from cells and tissue phantoms into human tissue. Once we confirmed contrast agent binding in biopsies, freshly resected oral tumors ( $n = 9$ ) were also incubated with the agent and analyzed. Patients gave written informed consent to participate, and the study was reviewed and approved by the institutional review boards at the University of Texas MD Anderson Cancer Center and Rice University. EGF–Alexa 647 (0.05 mg/ml concentration in 1× phosphate buffered saline, pH 7.4) was topically applied to these tissue samples in the presence of 10% dimethylsulfoxide (DMSO). DMSO was used as a permeation enhancer to improve delivery of the EGF–Alexa 647 conjugate through the epithelium of these tissue

samples [40,41]. Samples were incubated with EGF–Alexa 647 for 30 minutes, washed with 1× phosphate-buffered saline, and imaged using a wide-field fluorescence imaging system with appropriate excitation and emission filters. Wide-field imaging was used to survey the tissue because it has a large field of view ( $\sim 5 \times 7$  cm for these instruments). The biopsies were imaged with the CRiMaestro (Woburn, MA), a planar multispectral wide-field imaging device. The resected oral tumors were imaged with a multispectral digital microscope, consisting of a modified wide-field dental microscope capable of imaging in reflectance and fluorescence modes [42]. Appropriate control experiments were performed to ensure that data from these devices could be combined. To compare the increase in fluorescence intensity of incubated tissue, both preincubation and postincubation images were acquired. The preincubation image provided a measure of autofluorescence background from tissue. After wide-field imaging, the biopsy samples were sliced transversely to a thickness of 200 to 300  $\mu\text{m}$  and imaged in both reflectance (to locate epithelial and stromal regions of tissue slices) and fluorescence (to detect contrast agent) modes using a confocal microscope (Zeiss LSM 510). This high-resolution imaging was used to assess penetration depth

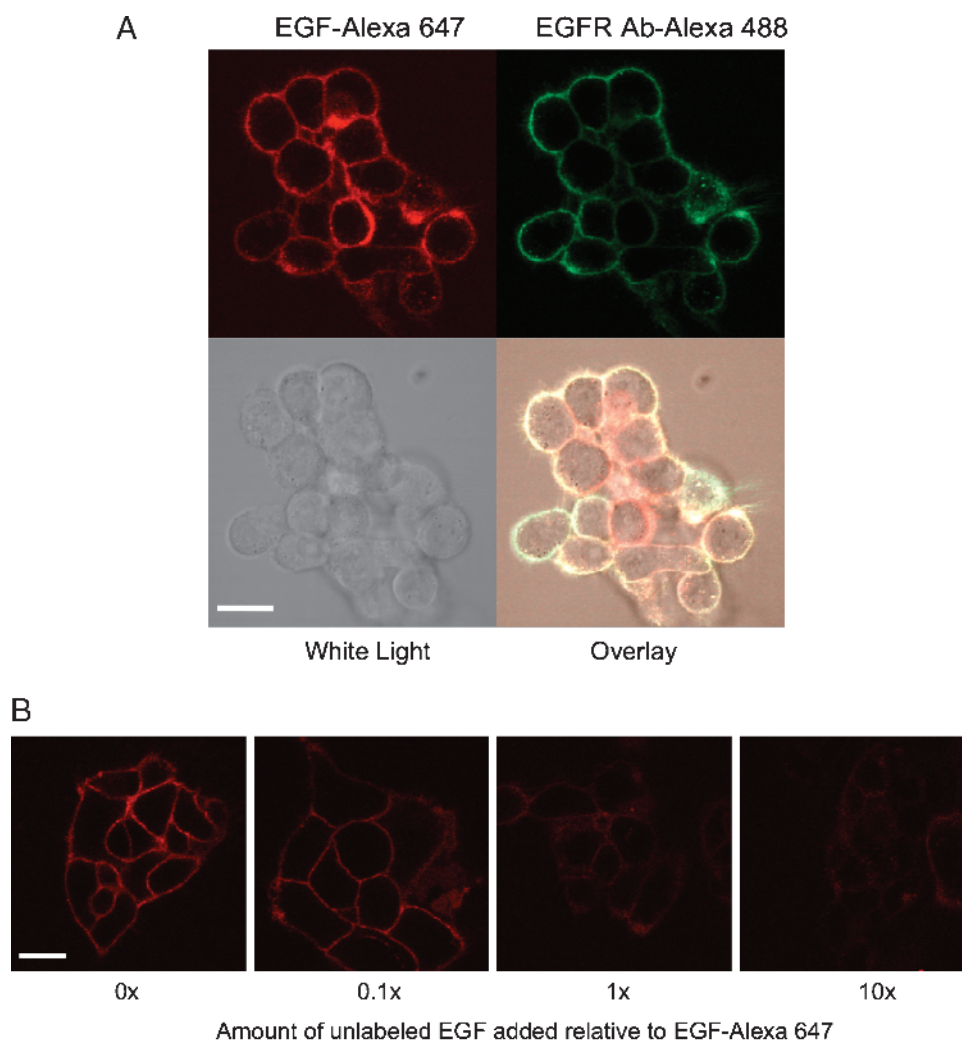


**Figure 1.** (A) EGFR-positive 1483 cells coincubated with EGF–Alexa 647 (red) and an anti–EGFR antibody labeled with Alexa 488 (green) showing colocalization of fluorescence at the cell membrane. Scale bar, 20  $\mu\text{m}$ . (B) Competition assay of 1483 cells incubated with EGF–Alexa 647 and unlabeled EGF added at concentrations of 0×, 0.1×, 1×, and 10× the amount of EGF–Alexa 647. Scale bar, 20  $\mu\text{m}$ .

of the EGF-dye conjugate. All tissue was returned to the Pathology Department of the University of Texas MD Anderson Cancer Center for hematoxylin and eosin staining and IHC processing. Immunohistochemical staining for EGFR was performed by the Research Histology Core Laboratory at MD Anderson Cancer Center following standard protocol with a standard EGFR antibody (clone 31G7 mouse antihuman; Zymed, South San Francisco, CA).

To further validate the specificity of EGF–Alexa 647 in oral tissues, a resected oral lesion was incubated with rhodamine-labeled 3-kDa dextran in 10% DMSO as a nonspecific fluorescent agent with a similar size as EGF peptide. The concentrations of fluorescently labeled dextran and incubation conditions were identical to the experiments performed with EGF–Alexa 647.

### Quantification of Imaging Data

Wide-field fluorescence images of the oral tissue samples obtained before and after incubation were quantitatively analyzed using Photoshop 7.0 to calculate the mean fluorescence intensity (MFI) across the tissue surface. A differential contrast value was calculated by finding the ratio of the increase in the MFI of neoplastic tissue after incubation relative to the increase in the MFI of normal tissue. For the biopsies, paired sets of abnormal and normal biopsies from the same patients were used together; for the resected oral lesions, a head and

neck surgical oncologist identified regions of clinically neoplastic and normal tissue from white light images of the lesions. The physician was blinded to the results of fluorescence imaging. Differential contrast was calculated for each clinical sample; results were compared with histology and IHC staining for EGFR.

Portions of the normal epithelium in the resected tumors displayed characteristics of hyperkeratosis or hyperplasia. Although these conditions are benign, they may affect the autofluorescence patterns and act as confounding factors in diagnostic strategies based on autofluorescence alone [43,44]. In addition, the thickened epithelium may result in entrapment of contrast agent, leading to artificially high differential contrast values. To investigate the specificity of the differential contrast approach with EGF–Alexa 647 and ensure that these conditions will not negatively affect our performance, differential contrast was calculated for regions of hyperkeratosis ( $n = 4$ ) and hyperplasia ( $n = 4$ ) as identified from histology slides by an expert head and neck pathologist. The epithelium in these regions was otherwise normal with no signs of dysplasia or cancer. Differential contrast was calculated for hyperkeratotic and hyperplastic regions relative to the same normal regions that were used previously; there was no overlap between these normal regions and regions of hyperkeratosis or hyperplasia. Differential contrast was also calculated for the tissue incubated with the rhodamine-labeled dextran as another control to investigate the specificity of EGF–Alexa 647.

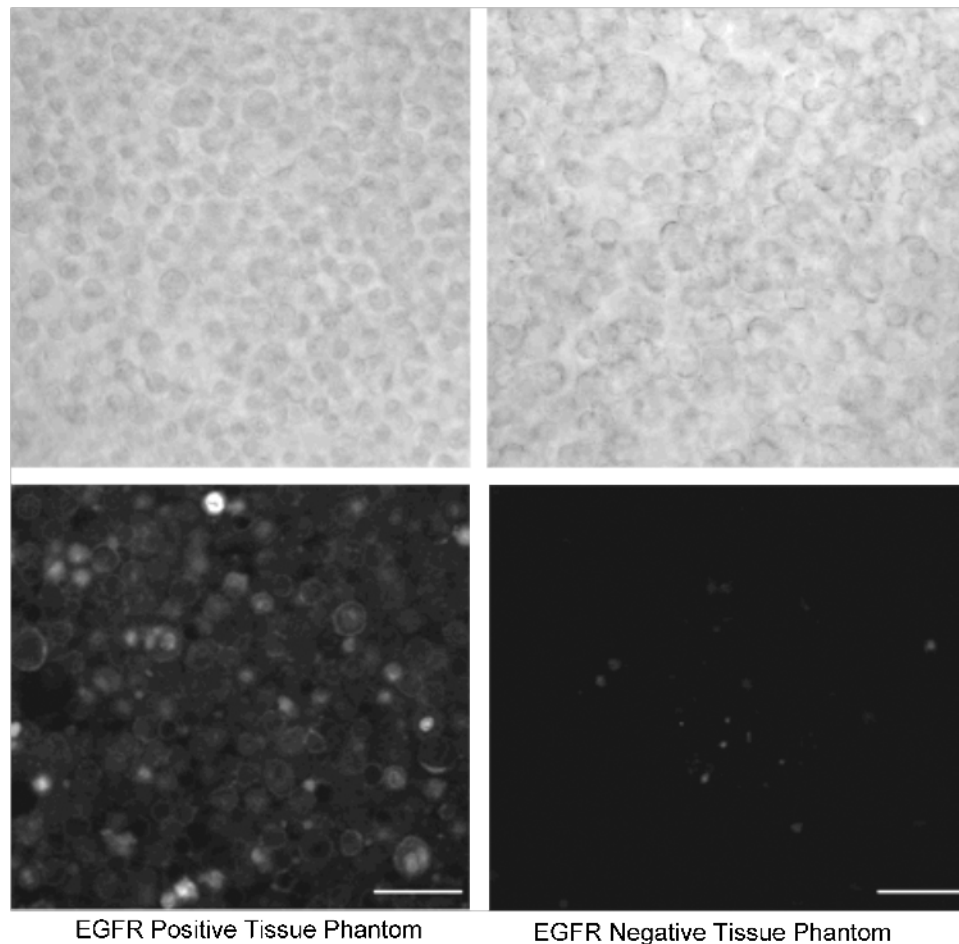


**Figure 2.** High-resolution white light and fluorescence confocal images of three-dimensional tissue culture phantoms incubated with the EGF–Alexa 647 conjugate. Scale bars, 100  $\mu\text{m}$ .

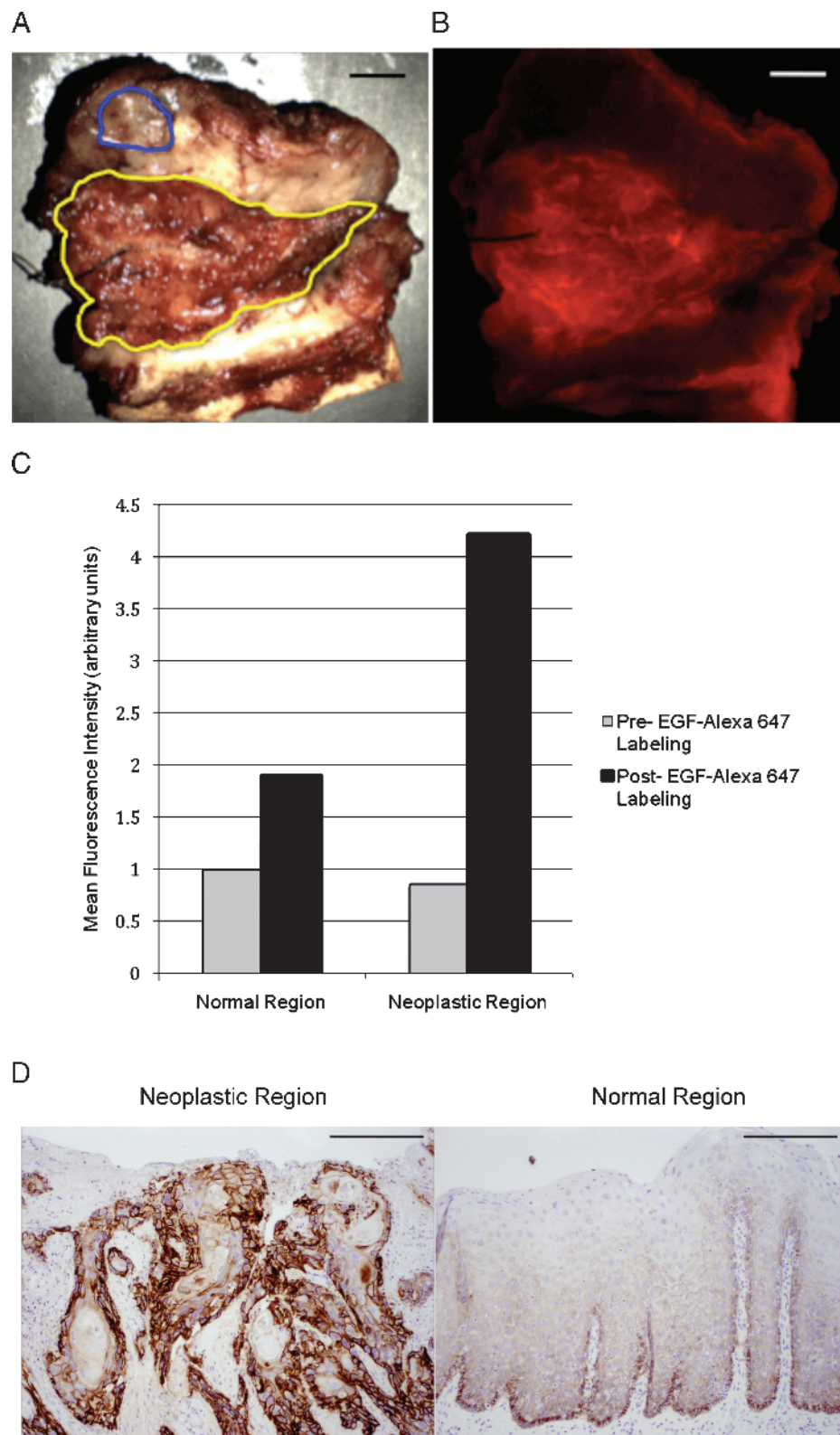
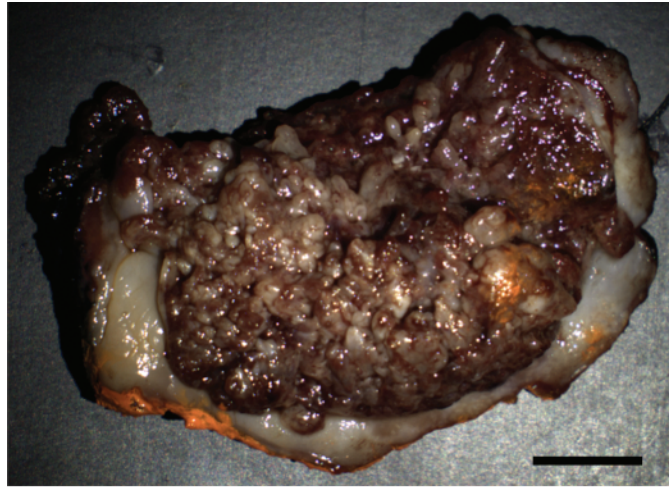


**Figure 3.** (A) Wide-field white light image of resected oral lesion. The neoplastic region as selected by an expert clinician blinded to the results of fluorescence imaging is outlined in yellow; the representative normal region is outlined in blue. The histologic diagnosis was invasive cancer. Scale bar, 1 cm. (B) Wide-field fluorescence image of the same sample obtained after topical delivery of EGF–Alexa 647 and washing to remove excess dye. Scale bar, 1 cm. (C) Mean fluorescence intensity of neoplastic and normal regions before and after incubation. All values are normalized to the intensity of the normal region before labeling. (D) EGFR IHC–stained sections from within the neoplastic and normal regions in the sample. Scale bars, 200  $\mu$ m.

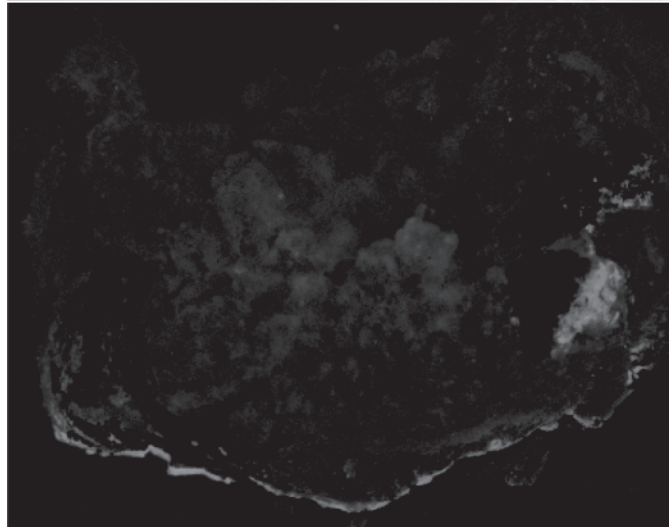
High-resolution confocal fluorescence images of biopsy slices incubated with EGF–Alexa 647 were also analyzed to quantitatively calculate the MFI in the epithelial region of normal and dysplastic samples and regions containing tumor cells for tumor specimens. A

radiometric contrast value was calculated for each set of paired biopsies by dividing the MFI of the clinically abnormal tissue by the MFI of the corresponding clinically normal sample. Results were compared with the histologic diagnosis of each biopsy set.

A)  
White Light



B)  
Post- incubation  
with rhodamine-  
labeled 3 kD  
dextran



C)  
Post- incubation  
with EGF-Alexa  
647

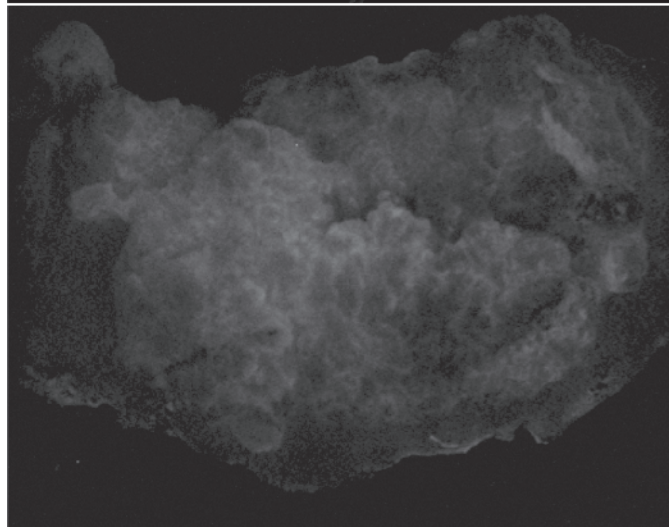


**Figure 4.** (A) Wide-field white light image of resected oral lesion. Scale bar, 1 cm. (B) Fluorescence image of tissue after incubating with rhodamine-labeled 3-kDa dextran. The orange pathology ink is the cause of fluorescence observed near the edges of the tissue. (C) Fluorescence image of tissue after incubating with EGF–Alexa 647.

## Results

Confocal fluorescence images of 1483 cells (EGFR-positive) incubated with the EGF–Alexa 647 conjugate showed bright red fluorescence localized at the cell membrane; in contrast, images of MDA-MB-435 cells (EGFR-negative) incubated with the agent did not show detectable signal under the imaging conditions used here (data not shown). The 1483 cells incubated with both EGF–Alexa 647 and anti-EGFR antibody labeled with Alexa 488 showed colocalization of fluorescence signal at the cell membrane as shown in Figure 1A. The competition assay with EGF–Alexa 647 and unlabeled EGF showed a decrease in fluorescence signal with increasing concentrations of unlabeled EGF as shown in Figure 1B. In addition, control experiments were also conducted using fluorescently labeled dextran. Images of cells incubated with rhodamine-labeled 3-kDa dextran did not show any binding to or retention of the nonspecific fluorescent agent in cells.

To evaluate whether the EGF–Alexa 647 conjugate could be delivered topically, initial experiments were carried out in three-dimensional tissue phantoms. Figure 2 shows confocal fluorescence images of two transversely sliced tissue phantoms that were incubated with EGF–Alexa 647 before slicing. Fluorescence signal was observed throughout the phantom containing the EGFR-positive 1483 cells, whereas no fluorescence signal was observed in the phantom containing the EGFR-negative 435 cells. In some of the 1483 cells, internalization of the contrast agent was observed. These results demonstrate that selective targeting of EGFR receptors can be achieved in this model system with topical delivery and that excess contrast agent can be easily removed with a simple washing step.

Next, EGF–Alexa 647 was topically delivered to fresh oral biopsies and resected lesions to demonstrate its ability to bind to human tissue. Figure 3A shows the white light wide-field image of a representative tissue sample with the clinically neoplastic region outlined in yellow and a representative normal region outlined in blue. Figure 3B shows the wide-field fluorescence image obtained after topical delivery of EGF–Alexa 647 and removal of excess contrast agent. A preincubation image was obtained using the same instrument parameters to estimate levels of autofluorescence signal from the tissue sample; the background autofluorescence at these wavelengths was very low. After incubating with the contrast agent, the fluorescence image shows greater fluorescence intensity in the neoplastic region compared with the normal region. Fluorescence observed on the edges of this specimen occurs as an artifact of surgical cautery. Fluorescence intensity of the representative normal region and the neoplastic region is shown quantitatively in Figure 3C, which compares the MFI before and after incubation of each region. Figure 3D shows the results of IHC staining for EGFR in tissue taken from neoplastic and normal regions. The results show strong staining indicating a high level of EGFR throughout the neoplastic region as compared with only weak staining localized to the basal layer of the epithelium indicating a low level of EGFR in the normal region. The IHC analysis is in agreement with the results from wide-field imaging on resected lesions. The pathological diagnosis for this representative case was invasive squamous cell carcinoma.

The resected oral lesion labeled with 3-kDa dextran as a nonspecific fluorescent agent is shown in Figure 4 in white light, after incubating with the rhodamine-labeled dextran, and after incubating with EGF–Alexa 647. Background fluorescence was subtracted using preincubation images. No visible nonspecific fluorescence is observed after incubating with dextran; after incubating with EGF–Alexa 647,

the neoplastic region shows bright fluorescence. The orange pathology ink on the tissue results in the fluorescence seen on the tissue edges in Figure 4B. Pathological diagnosis for this sample was invasive carcinoma.

A differential contrast value was calculated for each clinical sample to quantitatively compare fluorescence intensity increases in neoplastic and normal tissue. Figure 5 shows the differential contrast achieved for each specimen; the histopathologic diagnosis is also indicated. For samples with moderate to severe dysplasia ( $n = 4$ ), the differential contrast ranged from 1.6 to 3.9 with an average of 2.3. For samples with cancer ( $n = 13$ ), the differential contrast ranged from 2.0 to 6.9 with an average of 3.8.

To quantitatively examine the specificity of EGF–Alexa 647, regions of hyperkeratosis ( $n = 4$ ) and hyperplasia ( $n = 4$ ) were assessed for differential contrast value. The differential contrast obtained for these regions ranged from 0.8 to 1.2 with an average of 1.0. The contrast value of each region is also shown in Figure 5. To calculate a differential contrast value of the tissue incubated with dextran, images were taken at a long-enough exposure time to detect a fluorescence signal. The fluorescence at this higher exposure, however, was fairly homogenous, as indicated by the calculated differential contrast of 1.04. After incubating the tissue with EGF–Alexa 647, the differential contrast calculated (using the same regions of neoplastic and normal tissue) was 3.27.

After wide-field imaging of tissue samples, we obtained high-resolution confocal fluorescence images of transverse tissue slices prepared from biopsies incubated with EGF–Alexa 647. The aim of high-resolution imaging was to assess the tissue distribution of topically delivered EGF–Alexa 647 conjugate. Figure 6 shows images of a representative pair of biopsies after incubation. Figure 6A shows images (fluorescence and IHC) of a clinically abnormal sample diagnosed as cancer, whereas Figure 6B shows images of a clinically and histologically normal sample from the same patient. The fluorescence images highlight significant differences in the contrast agent signal of the two samples; the cancer specimen showed strong uniform

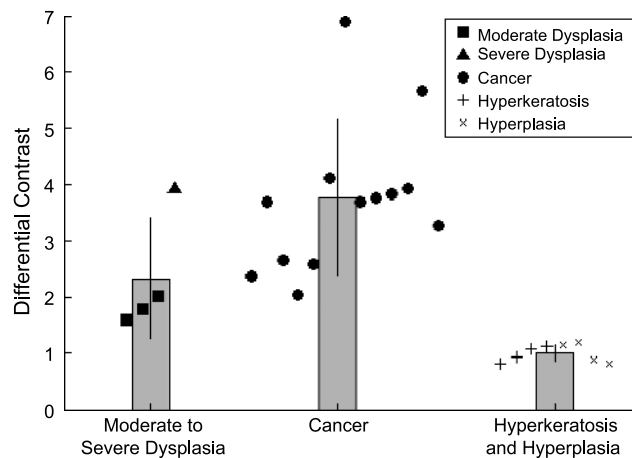


**Figure 5.** Differential contrast values calculated from wide-field fluorescence images of fresh oral tissue incubated with EGF–Alexa 647 conjugate. Each data point represents a pair of tissue specimens from a single patient. The bars represent the average differential contrast and SD for tissue with moderate to severe dysplasia ( $n = 4$ ) and tissue with cancer ( $n = 13$ ). Differential contrast values for regions of hyperkeratosis and hyperplasia ( $n = 8$ ) are also indicated.

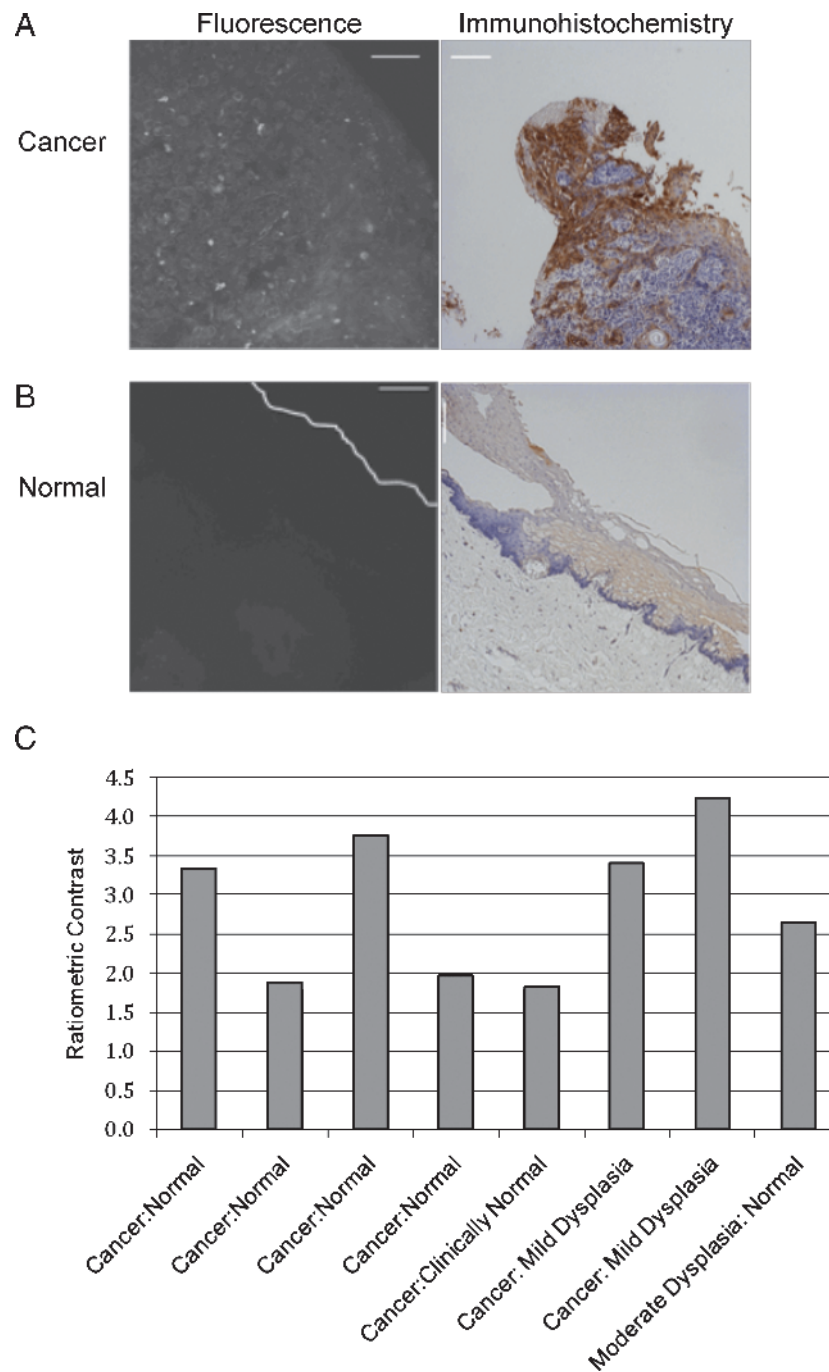


**Figure 6.** (A) Confocal fluorescence image and IHC image of a clinically abnormal specimen incubated with topically applied EGF–Alexa 647 conjugate. The histologic diagnosis was invasive cancer. Scale bars, 100  $\mu\text{m}$ . (B) Confocal fluorescence image and IHC image of a corresponding clinically and histologically normal specimen from the same patient incubated with topically applied EGF–Alexa 647 conjugate. The white line denotes the surface of the epithelium. Scale bars, 100  $\mu\text{m}$ . (C) Ratiometric contrast ratio calculated from high-resolution fluorescence images of eight biopsy pairs incubated with EGF–Alexa 647 conjugate. Histologic diagnosis is indicated for each pair.

fluorescence around epithelial cell membranes. In contrast, the normal sample shows only weak fluorescence around epithelial cells near the basement membrane. The images in Figure 6, *A* and *B*, demonstrate permeation of contrast agents to depths in excess of 500  $\mu\text{m}$ . No residual, nonspecific fluorescence was observed in these images, suggesting that excess fluorescent contrast agent can be removed with simple washing. The results of high-resolution optical imaging of EGFR expression in these clinical samples were validated using IHC analysis.

The IHC images show a strong expression of EGFR in the clinically abnormal biopsy but not in the corresponding normal sample.

A ratiometric contrast value was calculated for each set of paired biopsies ( $n = 8$  pairs) to quantitatively compare MFI from the high-resolution fluorescence images of these samples. The ratiometric contrast for each biopsy set is shown in Figure 6C; the histopathologic diagnosis is also indicated. The contrast is greater than 1.5 in all cases and ranges between two and four for most samples.

## Discussion

In this study, we evaluated the potential to image the expression of EGFR after topical delivery of fluorescently labeled EGF peptide for detection of oral neoplasia. We investigated the image contrast and topical delivery that could be achieved with this labeled peptide in both wide-field and high-resolution imaging, translating results from cells and tissue phantoms to intact human tissue specimens.

In wide-field fluorescence images of fresh oral tissue diagnosed as moderate or severe dysplasia, we observed an average 2.3-fold increase in the fluorescence signal in neoplastic tissue compared with normal tissue. For samples diagnosed as cancer, we observed an average 3.8-fold increase in fluorescence signal. The variability of differential contrast value between samples is expected because of patient-patient variability and differences in levels of EGFR expression in different sites within the oral cavity. We also observed some overlap in differential contrast values between dysplasia and cancer. Despite these variations, differential contrast values can distinguish neoplasia from normal tissue; every neoplastic sample had a contrast value greater than 1.5. Our calculated contrast values are consistent with previous studies, which have shown that EGFR expression level increases approximately two- to five-fold with the development of neoplasia. The increase in EGF–Alexa 647 staining intensity is also consistent with the degree of staining observed in IHC analysis.

Wide-field imaging observations of differential contrast are paralleled by high-resolution imaging observations of ratiometric contrast. Neoplastic oral biopsies showed a two- to four-fold higher fluorescence signal than paired normal biopsies. At the same time, normal specimens are associated with a small increase in fluorescence after topical application of EGF-dye. We attribute this change to two possible factors. The first is the basal level of EGFR in normal oral epithelium, which can contribute to the increase in fluorescence signal by specific targeting. Second, we observed entrapment of some fluorescence contrast agent in the keratinized superficial layer of some specimens. This entrapment of EGF-dye was observed in the case of a few biopsy specimens and could not be removed by simple washing steps. However, when differential contrast was calculated for regions of hyperkeratosis with underlying normal epithelium and in regions of hyperplasia, the average differential contrast value was 1.0, which would be expected for a normal region. All regions of hyperkeratosis or hyperplasia had contrast values lower than any regions with moderate to severe dysplasia or cancer. In this study, neoplastic samples are therefore consistently associated with higher EGF staining than normal samples, even those with a thickened keratin layer or thickened epithelium. Incubating tissue with the nonspecific fluorescent agent (rhodamine-labeled dextran) resulted in a differential contrast value of 1.04, which is significantly lower than any neoplastic sample. This result clearly demonstrates that EGF–Alexa 647 specifically targets neoplasia.

We selected the EGF peptide to target the EGF receptor rather than an anti-EGFR antibody, which has been used in previous studies to label transverse sections of tissue slices. The EGF peptide (~6 kDa) is significantly smaller than antibodies (~150 kDa), and owing to its small size, it has increased tissue permeability and clearance of unbound contrast agent can be achieved with simple washing steps. Topical delivery of EGF peptide-based contrast agents has the potential to overcome significant difficulties associated with targeting pre-invasive disease in oral tissue using IV delivery or subcutaneous injections. In IV-based delivery, the distribution of molecular contrast agents is controlled in large part by blood circulation. Because

the epithelial layer is avascular, direct delivery of contrast agents to epithelial cells is limited using IV delivery. In addition, losses during circulation, especially for small peptides, can further reduce the effective concentration [45]. IV-injected contrast agents typically require 24 to 48 hours of circulation time to achieve significant specific targeting of in tumor models. This significant delay can limit their use for screening. Further, many of the macromolecular contrast agents such as peptides are susceptible to degradation during such long incubation intervals [46].

One of the potential limitations in selecting naturally occurring growth factor ligands for molecular imaging applications is their ability to activate downstream cell signaling for proliferation. This observation has recently been reported using labeled human EGF peptide in implanted tumor cell lines [47]. To overcome this potential limitation, it is possible to select targeting peptides using library-based screening approaches. Studies have shown the potential to select EGFR targeting peptides with reduced proliferative activity compared with the natural EGF ligand [48,49].

A potential limitation of wide-field imaging alone is that it may be difficult to determine a precise margin of disease, especially if the tumor extends in the submucosa, because most photons collected with the current wide-field imaging device come from the superficial 3 mm of tissue. However, wide-field images are useful because they allow a quick survey of a large region of tissue and can be used to locate lesions and estimate disease margins. Even regions of moderate dysplasia that might not be obvious clinically displayed contrast agent binding that could be visualized with wide-field fluorescence imaging. Once an approximate margin is determined from wide-field images, high-resolution imaging can be used to refine this margin. Fiber-optic confocal systems can be placed on or inserted beneath the tissue surface to allow assessment of contrast agent binding to cells along the perimeter and therefore be used to determine a precise margin and detect submucosal tumor extension.

In summary, we have demonstrated noninvasive topical delivery of a molecular contrast agent to image changes in EGFR expression in oral neoplasia. Using a combination of wide-field and high-resolution imaging, we obtain quantitative contrast ratios to differentiate clinically neoplastic tissues from normal samples in both biopsies and resected oral lesions. The imaging results are in agreement with the pathological diagnosis as well as the IHC analysis. Results suggest that molecular imaging of EGFR is a noninvasive approach that may have the potential to aid in molecular diagnosis and characterization of oral neoplasia in a clinical setting.

## Acknowledgments

The authors thank Vivian Mack for providing help with cell cultures.

## Conflict of interest

Authors declare no conflict of interest.

## References

- [1] Gelovani Tjувajev J and Blasberg RG (2003). *In vivo* imaging of molecular-genetic targets for cancer therapy. *Cancer Cell* **3**, 327–332.
- [2] Massoud TF and Gambhir SS (2007). Integrating noninvasive molecular imaging into molecular medicine: an evolving paradigm. *Trends Mol Med* **13**, 183–191.
- [3] Pomper MG (2005). Translational molecular imaging for cancer. *Cancer Imaging* **5 Spec No A**, S16–S26.
- [4] Sokolov K, Aaron J, Hsu B, Nida D, Gillenwater A, Follen M, MacAulay C, Adler-Storthz K, Korgel B, Descour M, et al. (2003). Optical systems for *in vivo* molecular imaging of cancer. *Technol Cancer Res Treat* **2**, 491–504.

- [5] Weissleder R (2006). Molecular imaging in cancer. *Science* **312**, 1168–1171.
- [6] Bankfalvi A and Piffko J (2000). Prognostic and predictive factors in oral cancer: the role of the invasive tumour front. *J Oral Pathol Med* **29**, 291–298.
- [7] Chimenos-Kustner E, Font-Costa I, and Lopez-Lopez J (2004). Oral cancer risk and molecular markers. *Med Oral Patol Oral Cir Bucal* **9**, 381–384; 377–380.
- [8] Macluskey M and Ogden GR (2000). An overview of the prevention of oral cancer and diagnostic markers of malignant change: 2. Markers of value in tumour diagnosis. *Dent Update* **27**, 148–152.
- [9] Schliephake H (2003). Prognostic relevance of molecular markers of oral cancer—a review. *Int J Oral Maxillofac Surg* **32**, 233–245.
- [10] Banerjee AG, Bhattacharyya I, and Vishwanatha JK (2005). Identification of genes and molecular pathways involved in the progression of premalignant oral epithelia. *Mol Cancer Ther* **4**, 865–875.
- [11] Braakhuis BJ, Leemans CR, and Brakenhoff RH (2004). A genetic progression model of oral cancer: current evidence and clinical implications. *J Oral Pathol Med* **33**, 317–322.
- [12] Lippman SM, Sudbo J, and Hong WK (2005). Oral cancer prevention and the evolution of molecular-targeted drug development. *J Clin Oncol* **23**, 346–356.
- [13] Mankoff DA, Shields AF, and Krohn KA (2005). PET imaging of cellular proliferation. *Radiol Clin North Am* **43**, 153–167.
- [14] Muzi M, Mankoff DA, Grierson JR, Wells JM, Vesselle H, and Krohn KA (2005). Kinetic modeling of 3'-deoxy-3'-fluorothymidine in somatic tumors: mathematical studies. *J Nucl Med* **46**, 371–380.
- [15] Stokkel MR, ten Broek FW, and van Rijk PP (1998). The role of FDG PET in the clinical management of head and neck cancer. *Oral Oncol* **34**, 466–471.
- [16] Onizawa K, Saginoya H, Furuya Y, Yoshida H, and Fukuda H (1999). Usefulness of fluorescence photography for diagnosis of oral cancer. *Int J Oral Maxillofac Surg* **28**, 206–210.
- [17] Onizawa K, Okamura N, Saginoya H, and Yoshida H (2003). Characterization of autofluorescence in oral squamous cell carcinoma. *Oral Oncol* **39**, 150–156.
- [18] Betz CS, Stepp H, Janda P, Arbogast S, Grevers G, Baumgartner R, and Leunig A (2002). A comparative study of normal inspection, autofluorescence and 5-ALA-induced PPIX fluorescence for oral cancer diagnosis. *Int J Cancer* **97**, 245–252.
- [19] Leunig A, Betz CS, Mehlmann M, Stepp H, Arbogast S, Grevers G, and Baumgartner R (2000). Detection of squamous cell carcinoma of the oral cavity by imaging 5-aminolevulinic acid-induced protoporphyrin IX fluorescence. *Laryngoscope* **110**, 78–83.
- [20] McLoone N, Donnelly RF, Walsh M, Dolan OM, McLoone S, McKenna K, and McCarron PA (2008). Aminolaevulinic acid diffusion characteristics in “*in vitro*” normal human skin and actinic keratosis: implications for topical photodynamic therapy. *Photodermatol Photoimmunol Photomed* **24**, 183–190.
- [21] Frangioni JV (2006). Translating *in vivo* diagnostics into clinical reality. *Nat Biotechnol* **24**, 909–913.
- [22] Rumboldt Z, Day TA, and Michel M (2006). Imaging of oral cavity cancer. *Oral Oncol* **42**, 854–865.
- [23] Simon LL and Rubinstein D (2006). Imaging of oral cancer. *Otolaryngol Clin North Am* **39**, 307–317; vi.
- [24] Wilder-Smith P, Krasieva T, Jung WG, Zhang J, Chen Z, Osann K, and Tromberg B (2005). Noninvasive imaging of oral premalignancy and malignancy. *J Biomed Opt* **10**, 051601.
- [25] Veisheh M, Gabikian P, Bahrami SB, Veisheh O, Zhang M, Hackman RC, Ravanpay AC, Stroud MR, Kusuma Y, Hansen SJ, et al. (2007). Tumor paint: a chlorotoxin: Cy5.5 bioconjugate for intraoperative visualization of cancer foci. *Cancer Res* **67**, 6882–6888.
- [26] Ekberg T, Nestor M, Engstrom M, Nordgren H, Wester K, Carlsson J, and Anniko M (2005). Expression of EGFR, HER2, HER3, and HER4 in metastatic squamous cell carcinomas of the oral cavity and base of tongue. *Int J Oncol* **26**, 1177–1185.
- [27] Kuttan NA and Bhakthan NM (1997). Epidermal growth factor receptor (EGFR) in oral squamous cell carcinomas: overexpression, localization and therapeutic implications. *Indian J Dent Res* **8**, 9–18.
- [28] Richter P, Bohmer FD, Hindermann W, Borsi L, Hyckel P, Schleier P, Katenkamp D, Kosmehl H, and Berndt A (2005). Analysis of activated EGFR signalling pathways and their relation to laminin-5 gamma2 chain expression in oral squamous cell carcinoma (OSCC). *Histochem Cell Biol* **124**, 151–160.
- [29] Todd R and Wong DT (1999). Epidermal growth factor receptor (EGFR) biology and human oral cancer. *Histol Histopathol* **14**, 491–500.
- [30] Chen IH, Chang JT, Liao CT, Wang HM, Hsieh LL, and Cheng AJ (2003). Prognostic significance of EGFR and Her-2 in oral cavity cancer in betel quid prevalent area cancer prognosis. *Br J Cancer* **89**, 681–686.
- [31] Wahl MI and Carpenter G (1987). Role of growth factors and their receptors in the control of normal cell proliferation and cancer. *Clin Physiol Biochem* **5**, 130–139.
- [32] Perez-Soler R, Donato NJ, Shin DM, Rosenblum MG, Zhang HZ, Tornos C, Brewer H, Chan JC, Lee JS, Hong WK, et al. (1994). Tumor epidermal growth factor receptor studies in patients with non-small-cell lung cancer or head and neck cancer treated with monoclonal antibody RG 83852. *J Clin Oncol* **12**, 730–739.
- [33] Christensen ME, Engbaek F, Therkildsen MH, Bretlau P, and Nexø E (1995). A sensitive enzyme-linked immunosorbent assay used for quantitation of epidermal growth factor receptor protein in head and neck carcinomas: evaluation, interpretations and limitations. *Br J Cancer* **72**, 1487–1493.
- [34] Ishitoya J, Toriyama M, Oguchi N, Kitamura K, Ohshima M, Asano K, and Yamamoto T (1989). Gene amplification and overexpression of EGF receptor in squamous cell carcinomas of the head and neck. *Br J Cancer* **59**, 559–562.
- [35] Kawamoto T, Takahashi K, Nishi M, Kimura T, Matsumura T, and Taniguchi S (1991). Quantitative assay of epidermal growth factor receptor in human squamous cell carcinomas of the oral region by an avidin-biotin method. *Jpn J Cancer Res* **82**, 403–410.
- [36] Santini J, Formento JL, Francoual M, Milano G, Schneider M, Dassonville O, and Demard F (1991). Characterization, quantification, and potential clinical value of the epidermal growth factor receptor in head and neck squamous cell carcinomas. *Head Neck* **13**, 132–139.
- [37] Scambia G, Panici PB, Battaglia F, Ferrandina G, Almadori G, Paludetti G, Maurizi M, and Mancuso S (1991). Receptors for epidermal growth factor and steroid hormones in primary laryngeal tumors. *Cancer* **67**, 1347–1351.
- [38] Ang KK, Berkey BA, Tu X, Zhang HZ, Katz R, Hammond EH, Fu KK, and Milas L (2002). Impact of epidermal growth factor receptor expression on survival and pattern of relapse in patients with advanced head and neck carcinoma. *Cancer Res* **62**, 7350–7356.
- [39] Sokolov K, Galvan J, Myakov A, Lacy A, Lotan R, and Richards-Kortum R (2002). Realistic three-dimensional epithelial tissue phantoms for biomedical optics. *J Biomed Opt* **7**, 148–156.
- [40] De Rosa FS, Marchetti JM, Thomazini JA, Tedesco AC, and Bentley MV (2000). A vehicle for photodynamic therapy of skin cancer: influence of dimethylsulfoxide on 5-aminolevulinic acid *in vitro* cutaneous permeation and *in vivo* protoporphyrin IX accumulation determined by confocal microscopy. *J Control Release* **65**, 359–366.
- [41] Kurihara-Bergstrom T, Flynn GL, and Higuchi WI (1987). Physicochemical study of percutaneous absorption enhancement by dimethyl sulfoxide: dimethyl sulfoxide mediation of vidarabine (ara-A) permeation of hairless mouse skin. *J Invest Dermatol* **89**, 274–280.
- [42] Roblyer D, Richards-Kortum R, Sokolov K, El-Naggar AK, Williams MD, Kurachi C, and Gillenwater AM (2008). Multispectral optical imaging device for *in vivo* detection of oral neoplasia. *J Biomed Opt* **13**, 024019.
- [43] Muller MG, Valdez TA, Georgakoudi I, Backman V, Fuentes C, Kabani S, Laver N, Wang Z, Boone CW, Dasari RR, et al. (2003). Spectroscopic detection and evaluation of morphologic and biochemical changes in early human oral carcinoma. *Cancer* **97**, 1681–1692.
- [44] Pavlova I, Williams M, El-Naggar A, Richards-Kortum R, and Gillenwater A (2008). Understanding the biological basis of autofluorescence imaging for oral cancer detection: high-resolution fluorescence microscopy in viable tissue. *Clin Cancer Res* **14**, 2396–2404.
- [45] Lee SH, Lee S, Youn YS, Na DH, Chae SY, Byun Y, and Lee KC (2005). Synthesis, characterization, and pharmacokinetic studies of PEGylated glucagon-like peptide-1. *Bioconjug Chem* **16**, 377–382.
- [46] Powell MF, Grey H, Gaeta F, Sette A, and Colon S (1992). Peptide stability in drug development: a comparison of peptide reactivity in different biological media. *J Pharm Sci* **81**, 731–735.
- [47] Adams KE, Ke S, Kwon S, Liang F, Fan Z, Lu Y, Hirschi K, Mawad ME, Barry MA, and Sevick-Muraca EM (2007). Comparison of visible and near-infrared wavelength-excitable fluorescent dyes for molecular imaging of cancer. *J Biomed Opt* **12**, 024017.
- [48] Li K, Thomasson D, Ketali L, Contag C, Pomper M, Wright M, and Bray M (2005). Potential applications of conventional and molecular imaging to biodefense research. *Clin Infect Dis* **40**, 1471–1480.
- [49] Nakamura T, Takasugi H, Aizawa T, Yoshida M, Mizuguchi M, Mori Y, Shinoda H, Hayakawa Y, and Kawano K (2005). Peptide mimics of epidermal growth factor (EGF) with antagonistic activity. *J Biotechnol* **116**, 211–219.